

Quenched dynamics of two-dimensional solitons and vortices in the Gross-Pitaevskii equation

Qian-Yong Chen and P. G. Kevrekidis

Department of Mathematics and Statistics, University of Massachusetts, Amherst MA 01003-4515, USA

Boris A. Malomed

*Department of Physical Electronics, School of Electrical Engineering,
Faculty of Engineering, Tel Aviv University, Tel Aviv 69978, Israel*

We consider a two-dimensional (2D) counterpart of the experiment that led to the creation of quasi-1D bright solitons in Bose-Einstein condensates (BECs) [Nature **417**, 150–153 (2002)]. We start by identifying the ground state of the 2D Gross-Pitaevskii equation for repulsive interactions, with a harmonic-oscillator (HO) trap, and with or without an optical lattice (OL). Subsequently, we switch the sign of the interaction to induce interatomic attraction and monitor the ensuing dynamics. Regions of the stable self-trapping and catastrophic collapse of 2D fundamental solitons are identified in the parameter plane of the OL strength and BEC norm. The increase of the OL strength expands the persistence domain for the solitons to larger norms. For single-charged solitary vortices, in addition to the survival and collapse regimes, an intermediate one is identified, where the vortex resists the collapse but loses its structure, transforming into a fundamental soliton. The same setting may also be implemented in the context of optical solitons and vortices, using photonic-crystal fibers.

I. INTRODUCTION

The last decade has brought about a very substantial amount of research efforts in the physics of atomic Bose-Einstein condensates (BECs) [42, 43]. These studies have revealed a wide array of interesting phenomena, not only thanks to the precise control over experimental settings and the use of accurate and relatively simple theoretical models, which is a unique peculiarity of this area [12, 29], but also due to direct connections to other areas of physics, including superfluidity, superconductivity, quantum and nonlinear optics, and nonlinear wave theory.

One of the main topics for which these connections have been pursued is the study of the nonlinear dynamics of matter waves in BECs. Diverse experimental techniques have been used to produce a broad array of matter-wave excitations. In particular, phase engineering has been used to create vortices [36, 51] and dark solitons [4, 8, 13, 15, 16]. Stirring of the BECs has led to the formation of vortices [24, 32] and vortex-lattices [2, 3, 17]. The switch of the scattering length, from positive (repulsive) to negative (attractive), via Feshbach resonances, has been used to produce bright matter-wave solitons and soliton trains [11, 30, 46, 47]. These modes have been studied extensively, to the extent that numerous reviews (and even books [29]) are dedicated to bright solitons [1, 7], dark solitons [20] and vortices [18, 19, 26].

In this work, we aim to revisit a fundamental aspect associated with some of the principal experiments used to produce bright solitons, especially those carried out by the Rice group [46, 47]. (Note that a similar method was used for the creation of solitons in optical fibers in the pioneering works in that field [22, 35].) Precisely, we study the modulational instability (MI) [28] of the fundamental and vortex soliton after the *quench*, i.e., after switching the BEC system from repulsive to attractive interactions. While this mechanism was extremely efficient in the experimentally elaborated cigar-shaped setting, to the best of our knowledge it has not yet been systematically explored in quasi-two-dimensional (2D) pancake-shaped BECs. This is the subject of the present work, with emphasis on the formation of solitons and solitary vortices. More specifically, we examine the results of the sign switching of the nonlinearity from repulsive to attractive in the 2D BEC, trapped via a combination of a harmonic-oscillator (HO), i.e., magnetic, and periodic optical-lattice (OL) potentials [7, 40]. Our initial condition, prior to the quench, represents either the ground state of the system in the repulsive-interaction regime, or the dynamically stable excited state in the form of a vortex with topological charge $S = 1$ [18, 19, 26]. We note in passing that the vortex is stable in the case of the HO trap if its pivot is collocated with a local maximum of the OL potential, yet potentially unstable if is placed at a minimum [27, 31].

The paper is structured as follows. In section II, we introduce the model and some essential features of the numerical analysis. In section III, we report conclusions produced by the simulations for the fundamental solitons. A time-dependent variational approximation (VA) for this case is elaborated in section IV. In section V, the case of the solitary vortex is considered. A summary of the results and a discussion of possibilities for subsequent work are presented in section VI.

II. THE MODEL AND COMPUTATIONAL APPROACH

For sufficiently cold and dilute atomic gases, where the mean-field approximation is well-established, the BEC dynamics can be described by the mean-field order parameter (wave function), $\Psi(\mathbf{r}, t)$. Assuming a strongly anisotropic trap, with the transverse (x, y) and longitudinal (z) trapping frequencies chosen so that $\omega_x = \omega_y \equiv \omega_\perp \ll \omega_z$, the trapped BEC acquires a

nearly planar, (“pancake”) shape [29, 42, 43]. This, in turn, permits one to factorize the wave function, $\Psi = \Phi(z)\psi(x, y)$, where $\Phi(z)$ is the ground state of the respective HO. Next, averaging the underlying 3D Gross-Pitaevskii equation (GPE) equation along the longitudinal direction, z , leads to the following reduced (2D) GPE for the transverse component of the wave function (see also Refs. [29, 42, 43]):

$$i\hbar\partial_t\psi = -\frac{\hbar^2}{2m}\Delta\psi + g_{2D}|\psi|^2\psi + V_{\text{ext}}(x, y)\psi. \quad (1)$$

Here, $\Delta \equiv \partial_x^2 + \partial_y^2$ is the 2D Laplacian, m is the atomic mass, and $g_{2D} = g_{3D}/(\sqrt{2}\pi a_z)$ is an effective 2D coupling constant, where $g_{3D} \equiv 4\pi\hbar^2 a_s/m$ (a_s is the scattering length), and the longitudinal trapping length is $a_z = \sqrt{\hbar/m\omega_z}$. The potential $V_{\text{ext}}(x, y)$ in GPE (1) is a combination of the HO component and a 2D square-shaped OL:

$$\begin{aligned} V_{\text{ext}}(x, y) &= \frac{1}{2}m\omega_{\perp}^2 r^2 - \varepsilon[\cos^2(kx) + \cos^2(ky)] \\ &\equiv V_{\text{HO}}(r) + V_{\text{OL}}(x, y). \end{aligned} \quad (2)$$

Here, r is the radial variable, and the OL is characterized by its depth V_0 and periodicity $a_{\text{OL}} = \pi/k$. The wavenumber $k = (2\pi/\lambda) \sin(\theta/2)$ (i.e., $a_{\text{OL}} \equiv \lambda/(2 \sin(\theta/2))$), in turn, is controlled by the wavelength of the interfering beams that create the lattice and angle θ between them.

Measuring length in units of $a_{\text{OL}}/\pi \equiv 1/k$, time in units of $\omega_{\text{OL}} \equiv \hbar/E_{\text{OL}}$, and energy in units of $E_{\text{OL}} \equiv 2E_{\text{rec}} = \hbar^2/ma_{\text{OL}}^2$ (where E_{rec} is the lattice recoil energy), GPE (1) is cast into the following dimensionless form:

$$iu_t + \frac{1}{2}(u_{xx} + u_{yy}) + g|u|^2u - V_{\mathbf{x}}u = 0, \quad (3)$$

with potential

$$V_{\mathbf{x}} = \frac{1}{2}\Omega^2 r^2 - \varepsilon[\cos 2x + \cos 2y]. \quad (4)$$

In this normalized GPE, the wave function is rescaled as $\psi \rightarrow \sqrt{|g_{2D}|/E_{\text{OL}}}\psi \exp[i(V_0/E_{\text{OL}})t]$, and the sign parameter is $g \equiv \text{sign}(g_{\text{OL}}) = \pm 1$, with $g = -1$ and $g = +1$ corresponding respectively, to repulsive and attractive interatomic interactions. Further, the lattice depth in Eq. (4) is measured in units of $4E_{\text{rec}}$, while the normalized HO strength is $\Omega = a_{\text{OL}}^2/a_{\perp}^2 \equiv \omega_{\perp}/\omega_{\text{OL}}$, where $a_{\perp} = \sqrt{\hbar/m\omega_{\perp}}$ is the transverse trapping length.

We are interested in the dynamics of fundamental solitons and solitary vortices when the nonlinearity is switched from defocusing ($g < 0$) to focusing ($g > 0$). More precisely, we first fix $g = -1$ and solve the imaginary-time GPE version [10] to find the respective steady state for a given configuration, and then solve the GPE with $g = 1$, using that steady state as the initial condition. All the parameters stay the same except that g changes sign. In all the presented examples, $\Omega = 0.1$ is assumed in Eq. (4), yet our findings should be relevant to a wide range of Ω 's within the pancake setting.

Another way (a faster one) of finding such steady state that we employed is to plug ansatz $u = e^{-i\mu t}v(x, y)$ into Eq. (3) to derive a nonlinear eigenvalue problem, which is then solved with the Newton's method. Solutions produced by these two approaches are found to be virtually identical, with the maximum pointwise difference being between 10^{-8} and 10^{-10} for most configurations.

Unless specified otherwise, the Newton's solution is used as the initial condition in all the simulations. Further, the fourth-order split-step Fourier method [6, 39] is used to solve the GPE in time. The corresponding domain size is $[-8\pi, 8\pi] \times [-8\pi, 8\pi]$, with 256 Fourier modes in each direction and time step $\Delta t = 0.001$. The simulations were run up to $T = 2000$, which is large enough to observe the stability of the final states (if they are stable). Figure 1 shows some examples of the initial conditions, i.e., the steady states obtained by the Newton's method.

Control parameters will be the OL strength ε and the norm of the initial condition (i.e., the normalized number of atoms)

$$N = \int \int |u_0(x, y)|^2 dx dy. \quad (5)$$

The following main features of the solution will be computed: amplitude $(|u|)_{\text{max}}$, the final norm, which may be slightly different from the initial one due to radiation losses, and the total angular momentum,

$$M = (-i) \int \int \left(\frac{\partial u}{\partial \theta} u^* - \frac{\partial u^*}{\partial \theta} u \right) dx dy, \quad (6)$$

where θ is the angular coordinate. Note that M is conserved in the isotropic system that does not include the OL, and is not conserved with the presence of the OL. In particular, for isotropic solutions with integer vorticity S ,

$$u = e^{-i\mu t + iS\theta} U(r), \quad (7)$$

the relation between the angular momentum and norm is $M = 2SN$. We consider both the fundamental soliton with $S = 0$ and vortex soliton with topological charge $S = 1$, with or without the OL.

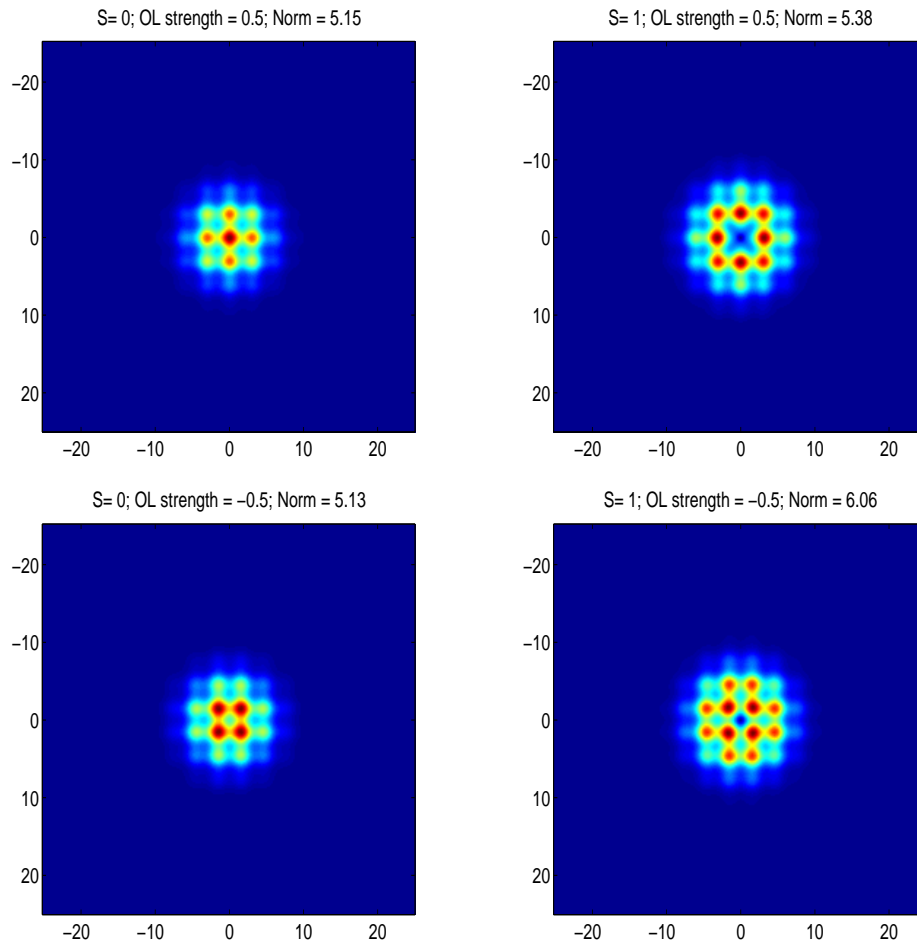


FIG. 1: (Color online) A typical example of the output produced by the Newton's method. Such states will be used as initial conditions in sections III and V. Left panels: $S = 0$ (fundamental solitons); right panels: $S = 1$ (vortices). Top and bottom panels correspond to $\varepsilon = 0.5$ and $\varepsilon = -0.5$, respectively.

III. GROUND-STATE QUENCH DYNAMICS

We start with the fundamental state with no topological charge. We perform the nonlinearity-sign switch (quench) for a wide range of OL strengths and initial norms. The former is used as a representative parameter associated with the potential, while the latter is employed for scanning through the set of initial data. The resulting two-dimensional map of the stability region of the ground state is plotted in Fig. 2. There are two regions with one denoted by open squares, wherein the ground state persists in the attractive regime in the form of a stable bright 2D soliton (see, e.g., Refs. [9, 23] for detailed discussions of the stability of such states), and the other denoted by filled circles, which corresponds to the catastrophic wave collapse, a well-known phenomenon for equations of the nonlinear-Schrödinger type [5, 48]. Clearly, the OL plays a critical role towards the stabilization the fundamental soliton, since the critical norm increases as the OL gets stronger. When the OL is absent ($\varepsilon = 0$), the soliton exhibits breathing dynamics when $N \leq 5.81$, and will collapse at $N > 5.91$. Note that the collapse threshold corresponding to the Townes soliton is $N_{\text{cr}} = 5.85$ [5].

In the presence of the OL, the dynamics is more complex, and in particular, the angular momentum will be generated when $\varepsilon < 0$. In such cases, the soliton's center initially coincides with a local maximum of the OL potential, hence it will slide down from this position. In fact, in the beginning of the simulation, the soliton moves back and forth between its initial position and the centers of other OL cells that are located along a straight line. (It is relevant to note that a 2D soliton can travel more than one cell, especially when the lattice is not very strong [45].) Then the soliton starts to deviate from this straight line at certain time, and the generation of the angular momentum commences. The subsequent motion does not follow any simple pattern. The trajectory of the soliton's center for one such case is shown in Fig. 3.

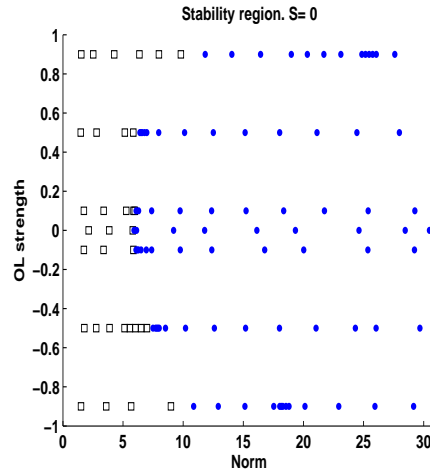


FIG. 2: (Color online) The stability diagram for the fundamental soliton resulting from the quench of the ground state of the repulsive BEC. The squares denote stable configurations that support breathing dynamics, while the dots denote unstable configurations that lead to the collapse.

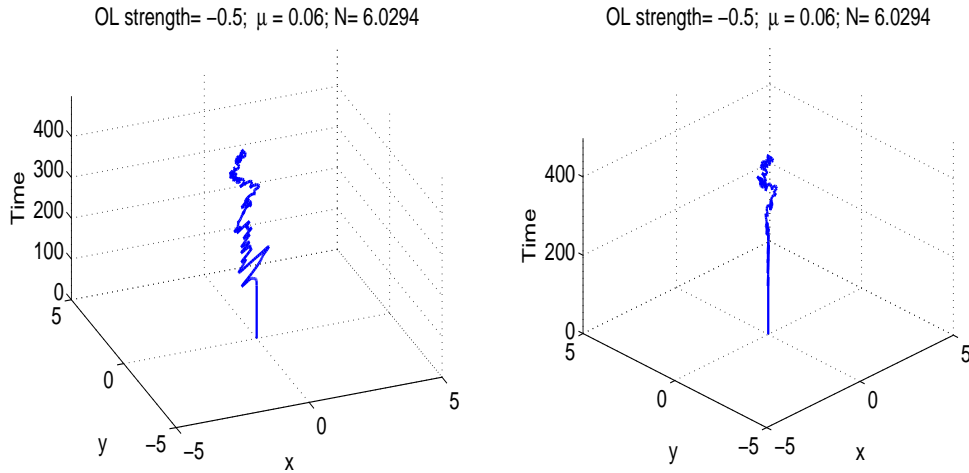


FIG. 3: (Color online) The trajectory of the soliton's center. The OL strength is $\varepsilon = -0.5$, while the soliton's parameters are $\mu = 0.06$, $N = 6.0294$. The left and right panels are shown from different angles to better represent the rather complex motion.

IV. THE VARIATIONAL APPROXIMATION

To develop an understanding of the breathing regime exhibited by the simulations, it is reasonable to apply the VA [33]. The starting point is the nonstationary GPE (3), but with a time-dependent nonlinearity coefficient $g(t)$. This equation can be derived from the Lagrangian, $L = \int_{-\infty}^{+\infty} dx \int_{-\infty}^{+\infty} dy \mathcal{L}(u)$, with density

$$\begin{aligned} \mathcal{L} = & \frac{i}{2} \left(\frac{\partial u}{\partial t} u^* - \frac{\partial u^*}{\partial t} u \right) - \frac{1}{2} \left(\left| \frac{\partial u}{\partial x} \right|^2 + \left| \frac{\partial u}{\partial y} \right|^2 \right) \\ & + \frac{g(t)}{2} |u|^4 + \left\{ -\frac{1}{2} \Omega^2 r^2 + \varepsilon [\cos(2x) + \cos(2y)] \right\} |u|^2. \end{aligned} \quad (8)$$

The variational *ansatz* for the fundamental state is based on the isotropic Gaussian,

$$u(r, t) = A(t) \exp \left(-\frac{r^2}{2W^2(t)} + \frac{1}{2} i b(t) r^2 + i \phi(t) \right), \quad (9)$$

where A , W , b and ϕ are, respectively, the amplitude, width, chirp and overall phase, which are assumed to be real functions of time. Following the standard procedure, we insert the *ansatz* into density (8) and calculate the corresponding effective

Lagrangian,

$$L_{\text{eff}} = 2\pi \int_0^\infty \mathcal{L} r dr. \quad (10)$$

The result of the calculation is

$$\begin{aligned} L_{\text{eff}} = & -N \frac{d\phi}{dt} - \frac{1}{2} N W^2 \frac{db}{dt} - \frac{N}{2W^2} - \frac{1}{2} N W^2 b^2 \\ & + \frac{N^2 g(t)}{4\pi W^2} - \frac{1}{2} \Omega^2 N W^2 + 2\epsilon N e^{-W^2}, \end{aligned} \quad (11)$$

where the overdot stands for the time derivative, and the norm of the ansatz is, cf. Eq. (5):

$$N \equiv \int_{-\infty}^{+\infty} dx \int_{-\infty}^{+\infty} dy |u(x, y)|^2 = \pi A^2 W^2. \quad (12)$$

The variational equation $\delta L_{\text{eff}}/\delta\phi = 0$ reproduces the conservation of the norm, $dN/dt = 0$, hence N may be treated as a constant. Then, equation $\delta L_{\text{eff}}/\delta b = 0$ yields an expression for the chirp:

$$b = \frac{1}{W} \frac{dW}{dt}, \quad (13)$$

and the final equation, $\delta L_{\text{eff}}/\delta(W^2) = 0$, leads to a closed-form evolution equation for the width, in which b is eliminated by means of Eq. (13):

$$\frac{d^2W}{dt^2} = \frac{2\pi - N g(t)}{2\pi W^3} - \Omega^2 W - 4\epsilon W e^{-W^2}. \quad (14)$$

For constant $g > 0$, Eq. (14) yields the well-known variational approximation for the critical norm, $N_{\text{cr}}^{(\text{var})} = 2\pi/g$ [14].

Aiming to compare results of the VA to those of the full simulations, we have to note that, as the initial profiles in the direct simulations were taken as per the steady state in the case with repulsive interactions, they are much wider than the OL cell. For this reason, the model including the OL cannot be adequately tackled by means of the (radially symmetric) ansatz (9), which does not include the density modulation induced by the OL. Therefore, the comparison is only carried out for the fundamental state in the absence of the OL.

A number of examples of the breathing regime of the resulting fundamental solitons are displayed in Fig. 4. These are obtained by solving Eq. (14), for which two initial conditions are needed. The first initial condition $W(t=0)$ is simply the width of the initial soliton, while the second initial condition $\frac{dW}{dt}(t=0)$ is approximated by a first order finite difference based on the widths of the solution in direction simulation at $t=0$ and $t=0.001$.

In Fig. 4, one observes that, for sufficiently small N , the resulting amplitude of the solution closely follows the VA prediction. However, as N increases, there arises a beating effect in the full GPE dynamics that is presumably not accounted for by the simplified VA dynamics of Eq. (14). Nevertheless, the VA still captures the principal features of the oscillatory dynamics of the width of the fundamental soliton.

V. THE QUENCH-INDUCED DYNAMICS OF VORTICES

With the introduction of initial vorticity, the most interesting observation is the rather delicate character of the stability of trapped solitary vortices under the self-attractive nonlinearity (see Ref. [38] and references therein). For the vortical initial inputs, we have performed an extensive numerical analysis similar to that reported in section III for the simpler case of the fundamental state. The respective two-parameter (the OL strength and initial norm) stability region is shown in Fig. 5. Here, we categorize both *coherent* and *less coherent* (see the examples below) states generated by the vortical inputs as stable when the collapse does not occur by $T = 2000$ (our *reporting horizon*). When $\epsilon = 0$ (i.e., the OL is absent), the critical norm for the quench process is found to be

$$N_{\text{cr}}^{(S=1)} \approx 11.81, \quad (15)$$

which is *essentially larger* than the known value, $N_{\text{max}}^{(S=1)} = 7.79$, i.e., the boundary of the existence of (numerically) exact stable trapped vortices with topological charge $S = 1$ [38]. Thus, the effective stability range of dynamical (breathing) vortices may be essentially broader than that of their static counterparts. For the simulation time exceeding $T = 2000$, the critical norm

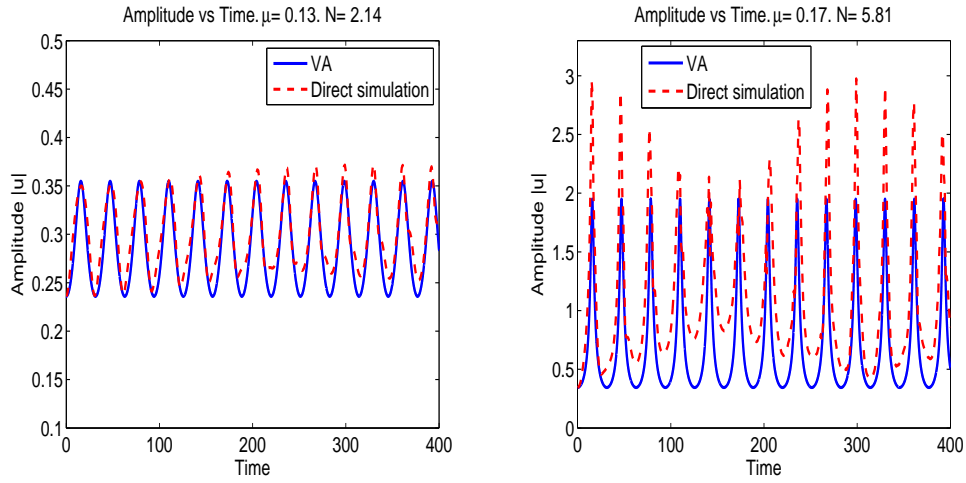


FIG. 4: (Color online) Comparison of the amplitude of the breathing fundamental soliton, generated by the quench, between the VA and direct simulations. The left panel refers to $N = 2.14$, and the right one to a vicinity of the critical point, for $N = 5.81$.

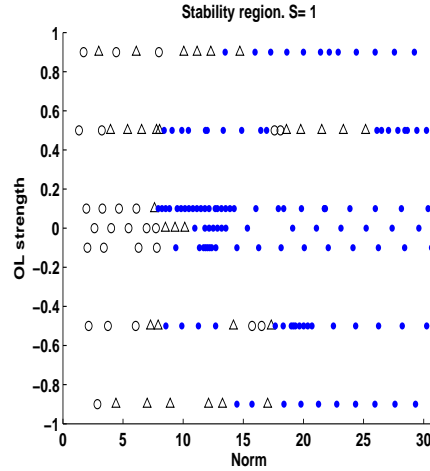


FIG. 5: (Color online) The stability region for the vortical initial condition with $S = 1$. Here, three regimes are identified. Circles represent the case when the resulting state is a vortex with charge $S = 1$. Triangles correspond to an intermediate regime of non-collapsing solutions, which, however, do not keep the vorticity. Finally, dots represent collapsing solutions.

may be found to vary slightly, as the stable solutions found at N very close to $N_{\text{cr}}^{(S=1)}$ are still in the process of splittings and recombinations at $T = 2000$. These "hesitating" solutions do not constitute a regular vortex soliton, but rather exhibit an additional breathing process.

The dynamics becomes much more complicated when the optical lattice is present. For these cases, the main conclusions are as follows.

(i) The stability region becomes smaller for a weak OL ($\varepsilon = \pm 0.1$). Yet, the stable solutions still behave like a coherent vortex ring, provided that norm N is not too large. With an increase of N , the solutions mimic the splitting-recombination scenario observed in the absence of the OL (see above). Two typical solutions are displayed in Fig. 6.

(ii) In the case of the OL with a moderate strength ($\varepsilon = \pm 0.5$), there are two regions in which the solution stays stable for up to $T = 2000$. In particular, it is stable when its initial norm lies in two intervals,

$$0 < N \leq 8.04, \quad (16)$$

$$17.59 \leq N \leq 25.17. \quad (17)$$

In the stability region (16), there are two kinds of solutions observed. When the norm is small enough, all the solutions are similar to the one shown in the top panel of Fig. 7. Basically, it is built of eight peaks forming two groups. The first group includes the peaks at the 3, 6, 9 and 12 o'clock positions, and this set is always present. The second group consists of the remaining peaks

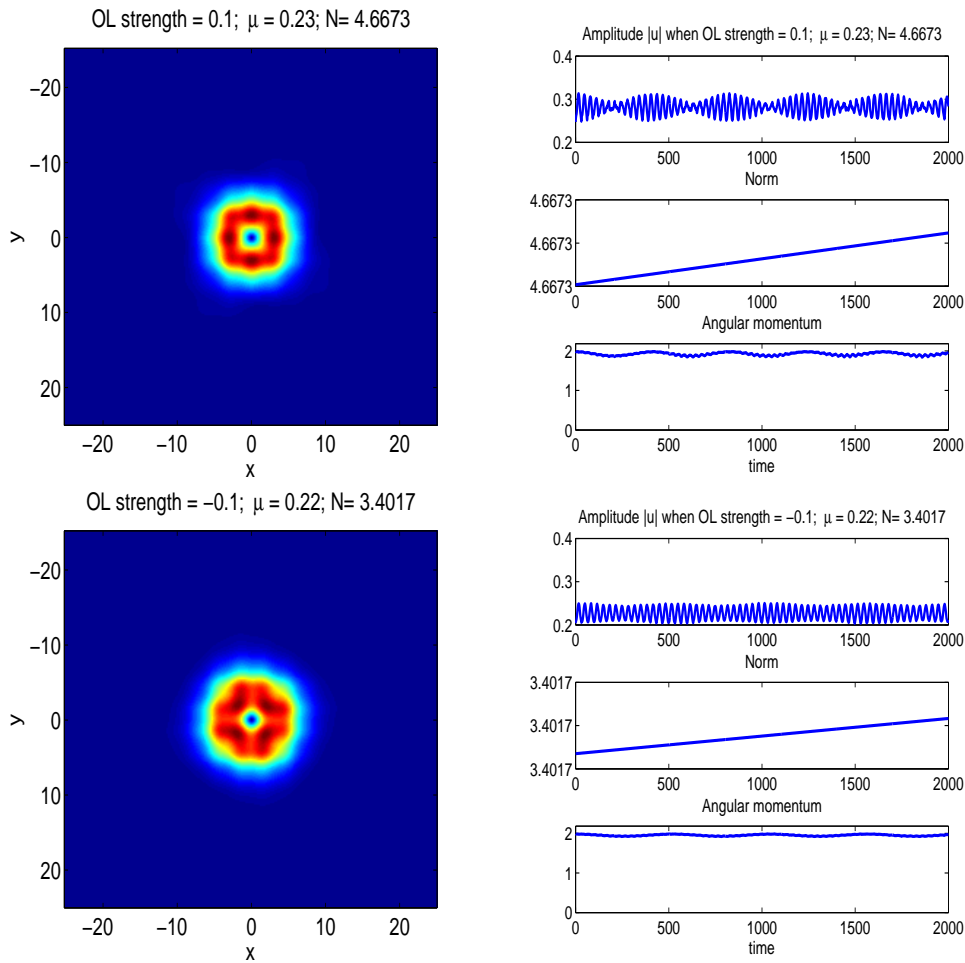


FIG. 6: (Color online) The dynamics of a typical stable vortex soliton with $S = 1$ in the presence of a weak OL. Top: $\varepsilon = 0.1$, $N = 4.6673$; bottom: $\varepsilon = -0.1$, $N = 3.4017$.

set along the diagonals, which breathe as a function of time (thus becoming more or less noticeable). The overall topological charge is still preserved [52]. The second kind of dynamics eventually leads to the loss of the vorticity, and transformation of the vortex into a fundamental soliton, as shown in the bottom panel of Fig. 7. Its location may vary, depending on the initial norm of the solution. The largest observed norm contained in such a stable peak is $N = 5.43$. When N is increased to be out of the stability region (16), the solution eventually collapses. In the stability region (17), the solutions for all the considered configurations feature four peaks. The largest total norm is $N = 21.53$, with 5.38 in each individual peak. A solution of this type is displayed at Fig. 8. However, only some of the stable solutions are true vortices (marked by circles in Fig. 5), bearing the topological charge of $S = 1$. For other solutions, the loss of the global coherence among the peaks occurs in the course of the evolution, at the same moment of time when the symmetry-breaking occurs, i.e., the peaks start to have different height. Two examples are presented in Fig. 9, with one preserving the vorticity (similar to the vortices on discrete lattice, although there is complete lack of the isotropy in the system [25, 34]), and one becoming incoherent and thus shedding the vorticity off.

(iii) For large strength of the OL (e.g., $\varepsilon = \pm 0.9$), the first stability region, corresponding to Eq. (16), expands, similar to what is the case for the fundamental states in Section III. On the other hand, the second stability region, which corresponds to Eq. (17), practically disappears. The final stable solutions (at $T = 2000$) exhibit breathing behavior. Yet aside from their more pronounced peaks, they do not exhibit any salient structural differences from their counterparts considered above at intermediate values of ε .

VI. CONCLUSIONS AND FUTURE CHALLENGES

In this work, we have examined the quenched dynamics of both the fundamental states and vortices with topological charge $S = 1$ in BEC. The quench consists of the sudden reversal of the nonlinearity sign from repulsive to attractive. The resulting

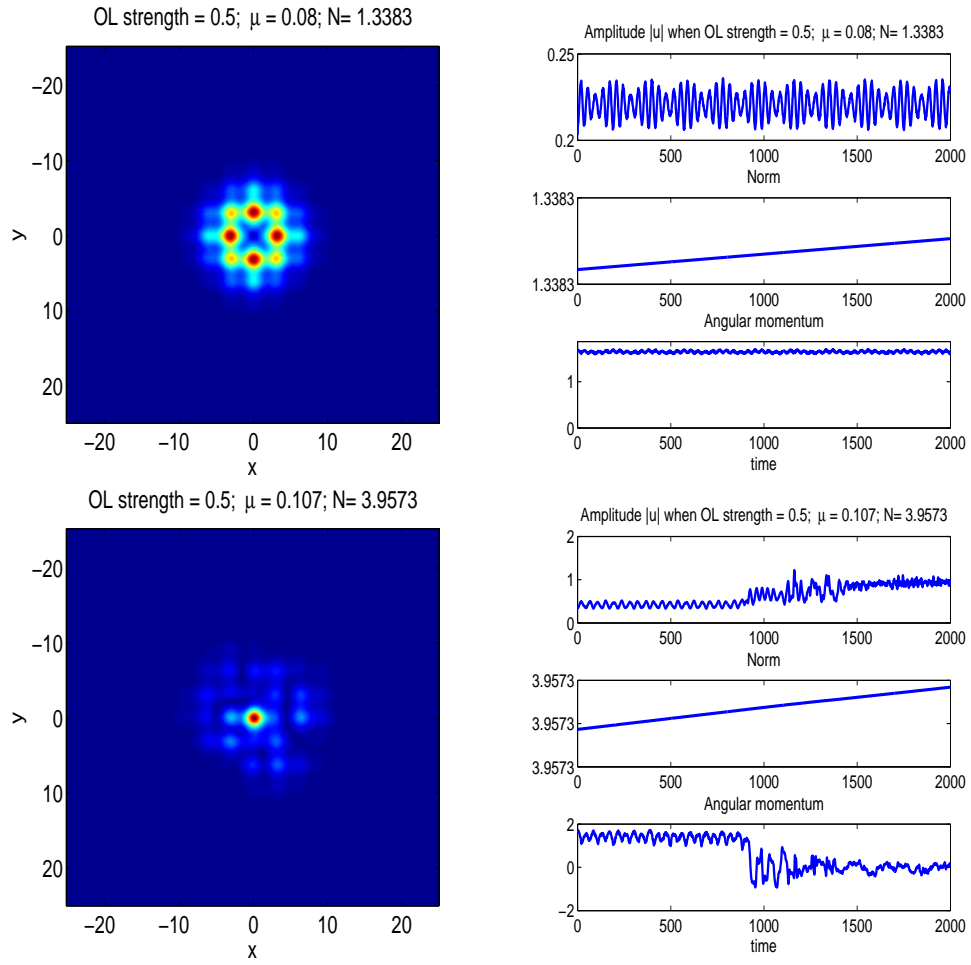


FIG. 7: (Color online) A vortex soliton with topological charge $S = 1$, for the OL strength $\varepsilon = 0.5$. Top: $N = 1.3383$, the final solution still being a vortex. Bottom: $N = 3.9573$, the solution evolving towards a fundamental soliton.

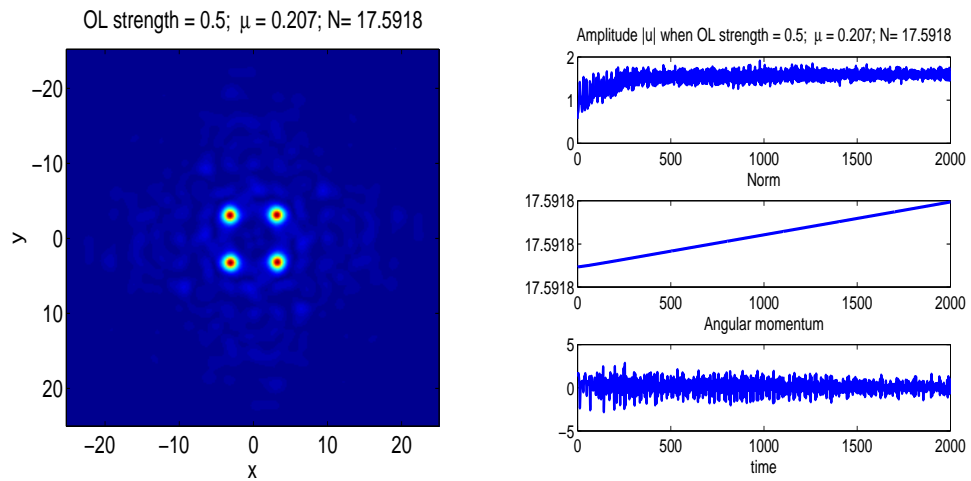


FIG. 8: (Color online) A vortex solution from the stability region (17). Here the lattice strength is $\varepsilon = 0.5$.

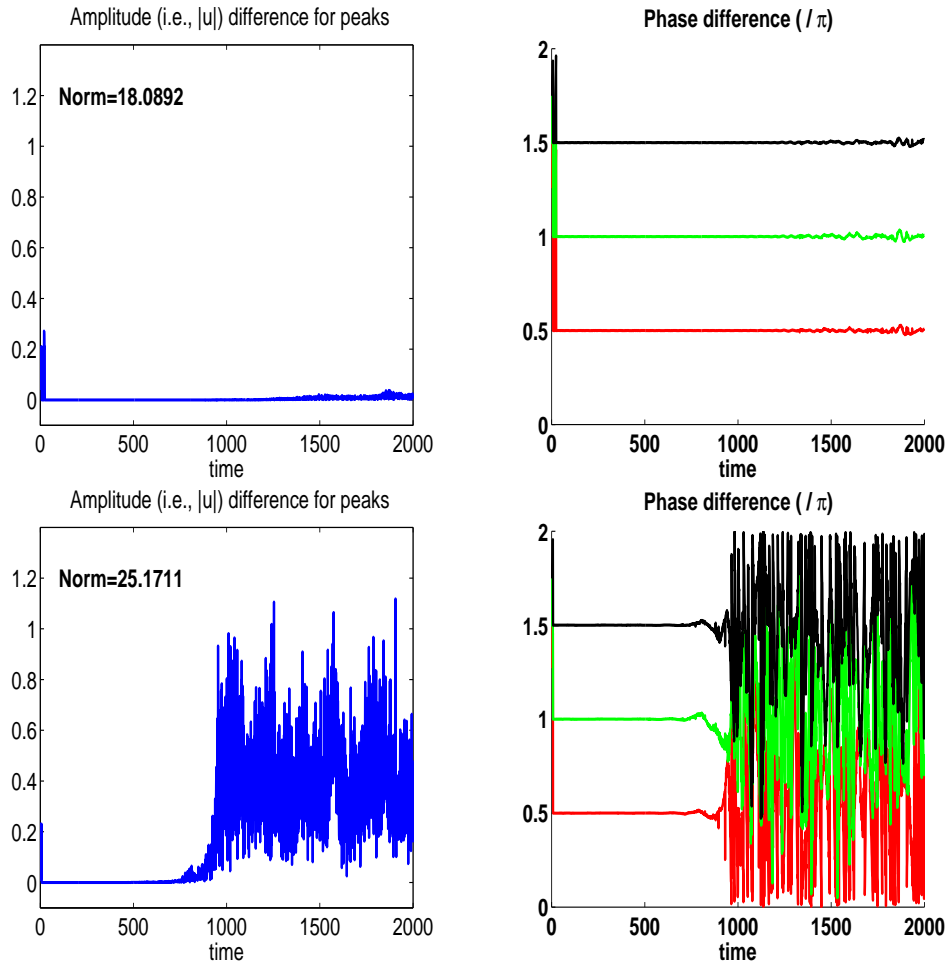


FIG. 9: (Color online) Examples of the loss of symmetry for the quasi-discrete vortices from the stability region (17). The OL strength is $\varepsilon = 0.5$. Left panels: the largest difference among the four peak amplitudes. Right panels: phase shifts (in units of π) between the peaks. Top: $N = 17.92$; bottom: $N = 25.17$.

states were investigated by systematic simulations, addressing both the impact of parameters, such as the strength of the OL (optical lattice), and the effect of initial conditions, by considering a range of values of the initial norm, N (which is proportional to the number of atoms in the BEC). A principal result is that the OL expands the range of initial norms which do not lead to the collapse of both the fundamental and vortex states. In fact, this expansion occurs well over the interval of norms for which static vortices were previously identified as stable states via the linear stability analysis. For the fundamental states, the application of the VA (variational approximation) is more efficient for the lower norm of the initial state. Additional beating effects, not captured by the VA, were found close to the collapse threshold. On the other hand, a particular finding, in the case of the vortex, is that, in addition to the regimes where a vortex survives in the breathing form or collapses, there is an intermediate regime where the vortex (in the presence of the OL) loses its topological character, yet remains immune to the collapse. Furthermore, a second stability region was identified for the vortex, in the presence of the OL with an intermediate strength, where the collapse was avoided due to the formation of a robust quasi-discrete vortex.

The same system may also be implemented in nonlinear optics, where the combination of the HO trap and OL potential corresponds to photonic-crystal fibers, while the switch of the nonlinearity corresponds to a junction of two waveguides made of self-defocusing and self-focusing materials [49].

We believe that these results provide a potential for further studies on this theme, both at the theoretical and at the experimental level. At the theoretical level, it may be useful to develop 3D generalizations of the analysis developed in this paper, either for the full case of spherically symmetric BECs or for strongly anisotropic traps. The effect of anisotropy in 2D would be interesting to examine too, as it departs from the configuration of the isotropic cylindrical trap. On the other hand, at the experimental level, recent advances in producing [41, 50] and monitoring [21, 37] the dynamics of vortices and vortex clusters, in conjunction with the well-established control of the BEC dynamics by means the Feshbach resonance [44], render particularly appealing and accessible examination of such quenches (or the corresponding adiabatic transitions) between the repulsive and attractive

regimes.

Acknowledgments. The work of Q.Y.C. was supported, in a part, by the National Science Foundation under the grant DMS-1016047. P.G.K. and B.A.M. appreciate a support provided by the Binational (US-Israel) Science Foundation through grant No. 2010239.

-
- [1] F. K. Abdullaev, A. Gammal, A. M. Kamchatnov, and L. Tomio. Dynamics of bright matter wave solitons in a Bose-Einstein condensate. *Int. J. Mod. Phys. B*, 19, 3415 (2005).
- [2] J. R. Abo-Shaer, C. Raman, and W. Ketterle. Formation and decay of vortex lattices in Bose-Einstein condensates at finite temperatures. *Phys. Rev. Lett.*, 88, 070409 (2002).
- [3] J. R. Abo-Shaer, C. Raman, J. M. Vogels, and W. Ketterle. Observation of vortex lattices in Bose-Einstein condensates. *Science*, 292:476–479, 2001.
- [4] B. P. Anderson, P. C. Haljan, C. A. Regal, D. L. Feder, L. A. Collins, C. W. Clark, and E. A. Cornell. Watching dark solitons decay into vortex rings in a Bose-Einstein condensate. *Phys. Rev. Lett.*, 86:2926–2929, 2001.
- [5] L. Bergé. Wave collapse in physics: principles and applications to light and plasma waves. *Phys. Rep.*, 303:259–372, 1998.
- [6] S. Blanes and P. C. Moan. Practical symplectic partitioned Runge-Kutta and Runge-Kutta-Nyström methods. *J. Comp. Appl. Math.*, 142:313–330, 2002.
- [7] V. A. Brazhnyi and V. V. Konotop. Theory of nonlinear matter waves in optical lattices. *Mod. Phys. Lett. B*, 18:627–651, 2004.
- [8] S. Burger, K. Bongs, S. Dettmer, W. Ertmer, K. Sengstock, A. Sanpera, G. V. Shlyapnikov, and M. Lewenstein. Dark solitons in Bose-Einstein condensates. *Phys. Rev. Lett.*, 83:5198–5201, 1999.
- [9] L. D. Carr and C. W. Clark. Vortices and ring solitons in Bose-Einstein condensates. *Phys. Rev. A*, 74, 043613 (2006).
- [10] M. L. Chiofalo, S. Succi, and M. P. Tosi. Ground state of trapped interacting Bose-Einstein condensates by an explicit imaginary-time algorithm. *Phys. Rev. E*, 62:7438–7444, 2000.
- [11] S. L. Cornish, S. T. Thompson, and C. E. Wieman. Formation of bright matter-wave solitons during the collapse of attractive Bose-Einstein condensates. *Phys. Rev. Lett.*, 96, 170401 (2006).
- [12] F. Dalfovo, S. Giorgini, L. P. Pitaevskii, and S. Stringari. Theory of Bose-Einstein condensation in trapped gases. *Rev. Mod. Phys.*, 71:463–512, 1999.
- [13] J. Denschlag, J. E. Simsarian, D. L. Feder, C. W. Clark, L. A. Collins, J. Cubizolles, L. Deng, E. W. Hagley, K. Helmerson, W. P. Reinhardt, S. L. Rolston, B. I. Schneider, and W. D. Phillips. Generating solitons by phase engineering of a Bose-Einstein condensate. *Science*, 287:97–101, 2000.
- [14] M. Desaix, D. Anderson, and M. Lisak. Variational approach to collapse of optical pulses. *J. Opt. Soc. Am. B*, 8:2082–2086, 1991.
- [15] Z. Dutton, M. Budde, C. Slowe, and L. V. Hau. Observation of quantum shock waves created with ultra-compressed slow light pulses in a Bose-Einstein condensate. *Science*, 293:663–668, 2001.
- [16] P. Engels and C. Atherton. Stationary and nonstationary fluid flow of a Bose-Einstein condensate through a penetrable barrier. *Phys. Rev. Lett.*, 99, 160405 (2007). arXiv:cond-mat/0704.2427.
- [17] P. Engels, I. Coddington, P. C. Haljan, and E. A. Cornell. Nonequilibrium effects of anisotropic compression applied to vortex lattices in Bose-Einstein condensates. *Phys. Rev. Lett.*, 89, 100403 (2002).
- [18] A. L. Fetter. Rotating trapped Bose-Einstein condensates. *Rev. Mod. Phys.*, 81:647–691, 2009.
- [19] A. L. Fetter and A. A. Svidzinsky. Vortices in a trapped dilute Bose-Einstein condensate. *J. Phys. Condens. Matter*, 13:R135–R194, 2001.
- [20] D. J. Frantzeskakis. Dark solitons in atomic Bose-Einstein condensates: from theory to experiments. *J. Phys. A: Math. Theor.*, 43, 213001 (2010).
- [21] D. V. Freilich, D. M. Bianchi, A. M. Kaufman, T. K. Langin, and D. S. Hall. Real-time dynamics of single vortex lines and vortex dipoles in a Bose-Einstein condensate. *Science*, 320, 1182 (2010).
- [22] A. Hasegawa. Generation of a train of soliton pulses by induced modulational instability in optical fibers. *Opt. Lett.*, 9:288–290, 1984.
- [23] G. Herring, L. D. Carr, R. Carretero-González, P. G. Kevrekidis, and D. J. Frantzeskakis. Radially symmetric nonlinear states of harmonically trapped Bose-Einstein condensates. *Phys. Rev. A*, 77, 023625 (2008).
- [24] S. Inouye, S. Gupta, T. Rosenband, A. P. Chikkatur, A. Görlitz, T. L. Gustavson, A. E. Leanhardt, D. E. Pritchard, and W. Ketterle. Observation of vortex phase singularities in Bose-Einstein condensates. *Phys. Rev. Lett.*, 87, 080402 (2001).
- [25] P. G. Kevrekidis. *The Discrete Nonlinear Schrödinger equation: Mathematical Analysis, Numerical Computations and Physical Perspectives*. Springer-Verlag, Heidelberg, 2009.
- [26] P. G. Kevrekidis, R. Carretero-González, D. J. Frantzeskakis, and I. G. Kevrekidis. Vortices in Bose-Einstein condensates: some recent developments. *Mod. Phys. Lett. B*, 18:1481–1505, 2004.
- [27] P. G. Kevrekidis, R. Carretero-González, G. Theocharis, D. J. Frantzeskakis, and B. A. Malomed. *J. Phys. B: At. Mol. Opt. Phys.*, 36:3467–3476, 2003.
- [28] P. G. Kevrekidis and D. J. Frantzeskakis. Pattern forming dynamical instabilities of Bose-Einstein condensates. *Mod. Phys. Lett. B*, 18:173–202, 2004.
- [29] P. G. Kevrekidis, D. J. Frantzeskakis, and R. Carretero-González (eds.). *Emergent nonlinear phenomena in Bose-Einstein condensates. Theory and experiment*. Springer-Verlag, Berlin, 2008.
- [30] L. Khaykovich, F. Schreck, G. Ferrari, T. Bourdel, J. Cubizolles, L. D. Carr, Y. Castin, and C. Salomon. Formation of a matter-wave bright soliton. *Science*, 296:1290–1293, 2002.

- [31] K. J. H. Law, L. Qiao, P. G. Kevrekidis, and I. G. Kevrekidis. Stability of quantized vortices in a Bose-Einstein condensate confined in an optical lattice. *Phys. Rev. A*, 77: 053612 (2008).
- [32] K. W. Madison, F. Chevy, W. Wohlleben, and J. Dalibard. Vortex formation in a stirred Bose-Einstein condensate. *Phys. Rev. Lett.*, 84:806–809, 1999.
- [33] B. A. Malomed. Variational methods in nonlinear fiber optics and related fields. In E. Wolf, editor, *Progress in Optics*, volume 43, pages 71–193. North-Holland, 2002.
- [34] B. A. Malomed and P. G. Kevrekidis. Discrete vortex solitons. *Phys. Rev. E*, 64: 026601 (2001).
- [35] P. V. Mamyshev, S. V. Chernikov, and E. M. Dianov. Generation of fundamental soliton trains for high-bit-rate optical fiber communication lines. *IEEE J. Quant. Electr.*, 27:2347–2355, 1991.
- [36] M. R. Matthews, B. P. Anderson, P. C. Haljan, D. S. Hall, C. E. Wieman, and E. A. Cornell. Vortices in a Bose-Einstein condensate. *Phys. Rev. Lett.*, 83:2498–2501, 1999.
- [37] S. Middelkamp, P. J. Torres, P. G. Kevrekidis, D. J. Frantzeskakis, R. Carretero-González, P. Schmelcher, D. V. Freilich, and D. S. Hall. Guiding-center dynamics of vortex dipoles in Bose-Einstein condensates. *Phys. Rev. A*, 84: 011605 (2011).
- [38] D. Mihalache, D. Mazilu, B. A. Malomed, and F. Lederer. Vortex stability in nearly-two-dimensional Bose-Einstein condensates with attraction. *Phys. Rev. A*, 73: 043615 (2006).
- [39] G. D. Montesinos and V. M. Pérez-García. Numerical studies of stabilized townes solitons. *Math. Comput. Simulat.*, 69:447–456, 2005.
- [40] O. Morsch and M. Oberthaler. Dynamics of Bose-Einstein condensates in optical lattices. *Rev. Mod. Phys.*, 78:179–215, 2006.
- [41] T. W. Neely, E. C. Samson, A. S. Bradley, M. J. Davis, and B. P. Anderson. Observation of vortex dipoles in an oblate Bose-Einstein condensate. *Phys. Rev. Lett.*, 104: 160401 (2010).
- [42] C. J. Pethick and H. Smith. *Bose-Einstein Condensation in Dilute Gases*. Cambridge University Press, Cambridge, 2001.
- [43] L. Pitaevskii and S. Stringari. *Bose-Einstein Condensation*. Oxford University Press, Oxford, 2003.
- [44] S. E. Pollack, D. Dries, M. Junker, Y. P. Chen, T. A. Corcovilos, and R. G. Hulet. Extreme tunability of interactions in a ^7Li Bose-Einstein condensate. *Phys. Rev. Lett.*, 102: 090402 (2009).
- [45] H. Sakaguchi and B. A. Malomed. Two-dimensional loosely and tightly bound solitons in optical lattices and inverted traps. *J. Phys. B*, 37:2225–2239, 2004.
- [46] K. E. Strecker, G. Partridge, A. G. Truscott, and R. G. Hulet. Bright matter wave solitons in Bose-Einstein condensates. *New J. Phys.*, 5: 73 (2003).
- [47] K. E. Strecker, G. Partridge, A. G. Truscott, and R. G. Hulet. Formation and propagation of matter-wave soliton trains. *Nature*, 417:150–153, 2002.
- [48] C. Sulem and P. L. Sulem. *The Nonlinear Schrödinger Equation*. Springer-Verlag, New York, 1999.
- [49] I. Towers and B. A. Malomed. Stable (2+1)-Dimensional solitons in a layered medium with sign-alternating Kerr nonlinearity. *J. Opt. Soc. Am.*, 19:537–543, 2002.
- [50] C. N. Weiler, T. W. Neely, D. R. Scherer, A. S. Bradley, M. J. Davis, and B. P. Anderson. Spontaneous vortices in the formation of Bose-Einstein condensates. *Nature*, 455:948–951, 2008.
- [51] J. E. Williams and M. J. Holland. Preparing topological states of a Bose-Einstein condensate. *Nature*, 401:568–572, 1999.
- [52] A video illustrating this case can be found at: http://www.math.umass.edu/~qchen/S1_OLE05_N1.zip